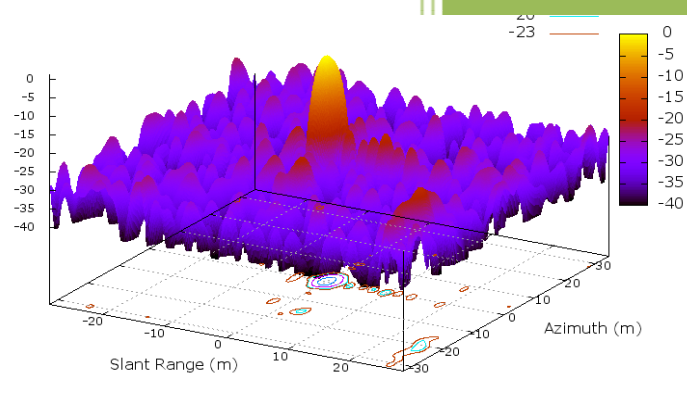
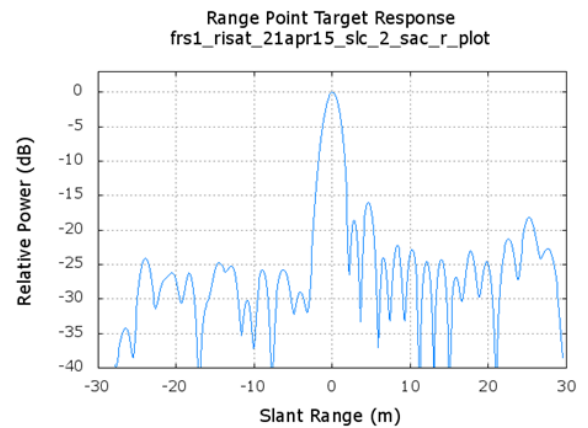
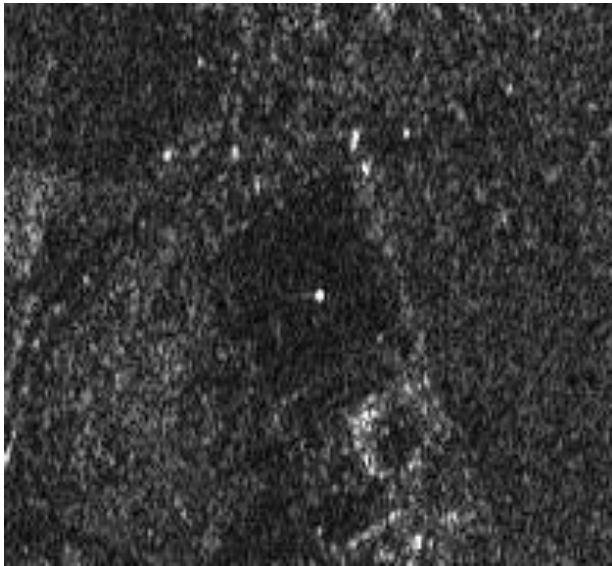




Absolute Calibration and image quality assessment of RISAT-1 FRS and MRS mode data



CAL-VAL Team

Space Applications Centre-ISRO

September 2015

DOCUMENT CONTROL SHEET

1. Report No.	SAC/EPESA/ADVG/CVD/CAL-VAL/SR/01/09/2015
2. Publication date	September 2015
3. Title and subtitle	Absolute Calibration and image quality assessment of RISAT-1 FRS and MRS mode data
4. Type of report	Scientific
5. Number of pages	25
6. Number of references	32
7. Authors	CAL-VAL Team
8. Originating unit	CVD-ADVG-EPESA
9. Abstract	In this work, absolute radiometric calibration of RISAT-1 MRS and FRS mode HH polarization data has been done. Two dates (21 st April and 25 th April 2015) FRS with beam number 104 and 21 and two dates MRS (5 th July 2015 and 30 th July 2105) data have been used in the study. Calibration was done by utilizing the point target (corner reflectors). The impulse response functions of the deployed corner reflectors were studied and data quality parameters have also been computed using the point target IRF.
10. Key words	Corner reflector, Corner reflector Deployment, Impulse Response Function, Calibration Constant, Backscattering Coefficient
11. Security classification	Unrestricted
12. Distribution statement	General

CAL-VAL Team

1. Space Applications Centre (SAC-ISRO), Ahmedabad

Dr. A K Mathur- Coordinator

Mr. R.J. Prajapati- Co-Principal Investigator

Mrs. Shweta Sharma- Principal Investigator

2. Nirma University, Ahmedabad

Dr. P R Patel- Co-Principal Investigator

Mr. Gautam Dadhich- Junior Research Fellow

Table of Contents

1.0 Introduction	
1.1 Need of Calibration.....	1
1.2 RISAT-1 SAR Sensor.....	2
2.0 Theoretical background	4
3.0 Study Area and Data sets	10
4.0 Methodology	12
5.0 Results and Discussions	14
6.0 Future Work	21
Acknowledgements	22
References	23-25

1.0 Introduction

Synthetic Aperture Radar (SAR) was first developed in the 1950's [1], for long-range mapping from airborne platforms. As the popularity of the SAR increased several space agencies started focussing on it and in the present scenario, different space agencies throughout the world have already launched their own spaceborne SAR sensor into orbit [2]-[7] including India's own satellite RISAT-1 with SAR Sensor [8: Current Science] , and airborne SAR's for remote sensing abound. The new generation of SAR sensors is designed to be operationally stable, equipped with capabilities such as multifrequency, multipolarization data-gathering, interferometric modes, and wide-swath coverage. The list of applications for SAR as a remote sensing tool is also rapidly expanding in fields as diverse as oceanography, forestry, sea-ice monitoring, planetary exploration, geology, agriculture, and terrain mapping.

The major goal in utilizing imaging radar data is to infer some bio- or geophysical parameter about target areas within the scene via analysis of the recorded radar signal. For coherent radar systems such as a synthetic aperture radar (SAR), the recorded signal consists of both phase and amplitude information. Although many applications like InSAR, PolInSAR require extraction of phase information from SAR data, a majority of applications utilize the amplitude information recorded in the SAR signal history. To utilize this amplitude information requires a normalization process to remove radar system effects. This normalization process usually results in an estimate of the radar cross section (σ) or scattering coefficient (σ_0) on a pixel-by-pixel basis for the various targets being imaged by the radar and is referred to as radiometric calibration.

1.1 Need of Calibration

Use of Synthetic Aperture Radar (SAR) imagery for any application which involves comparative temporal or spatial study of the radar reflectivity of extended areas, e.g., in forestry, agriculture, or hydrology, depends to a large extent on the ability to radiometrically calibrate the imagery [9]. For any quantitative analysis radiometrically calibrated data is required. With radiometrically calibrated data it is possible to compare values obtained by one SAR sensor to that obtained by other SAR sensors and also to ground based observations. Thus it will be helpful to extend results of studies carried out using one sensor to other. Ideally, calibration should be "absolute" so that results from different systems may be compared with each other and with theoretical models for the terrain backscatter coefficient. For a given SAR image, the digital number (DN) is proportional to the received voltage. Therefore the image intensity is proportional to the received power. The process to retrieve

SAR backscattering coefficient from the observed image intensity is known as radiometric calibration. Over a period of time, need of radiometric calibration has become absolutely necessary in view of availability of SAR data from various spaceborne sensors like ERS-1/2, Envisat, Radarsat-1/2, ALOS PALSAR-1/2, CosmoSkymed, TerraSAR-X and RISAT-1.

To compare data from different sensors, extract geophysical parameters from backscatter measurements using models, carrying out multi-temporal studies over large areas, build up a database of backscatter measurements for different types of terrain/incidence angle, etc., requires calibrated SAR data products. Thus the present study focuses on the radiometric calibration of RISAT-1 SAR sensor for passive standard target.

1.2 RISAT-1 SAR Sensor

RISAT-1 is India's first space borne SAR sensor operating at C band. RISAT-1 is not only capable of acquiring data in multi polarisation mode, including quad linear polarisation, but it is also first of its kind to operate in hybrid circular polarimetric mode for earth observation [8:CS]. It operates at various beam modes having a number of combinations of linear polarisation modes as well as circular polarisation modes, incidence angle, swath and resolution. Fig.1 shows schematic diagram of RISAT-1 SAR beam modes [10]. Detailed specifications of RISAT-1 SAR beam modes are given in Table-1.

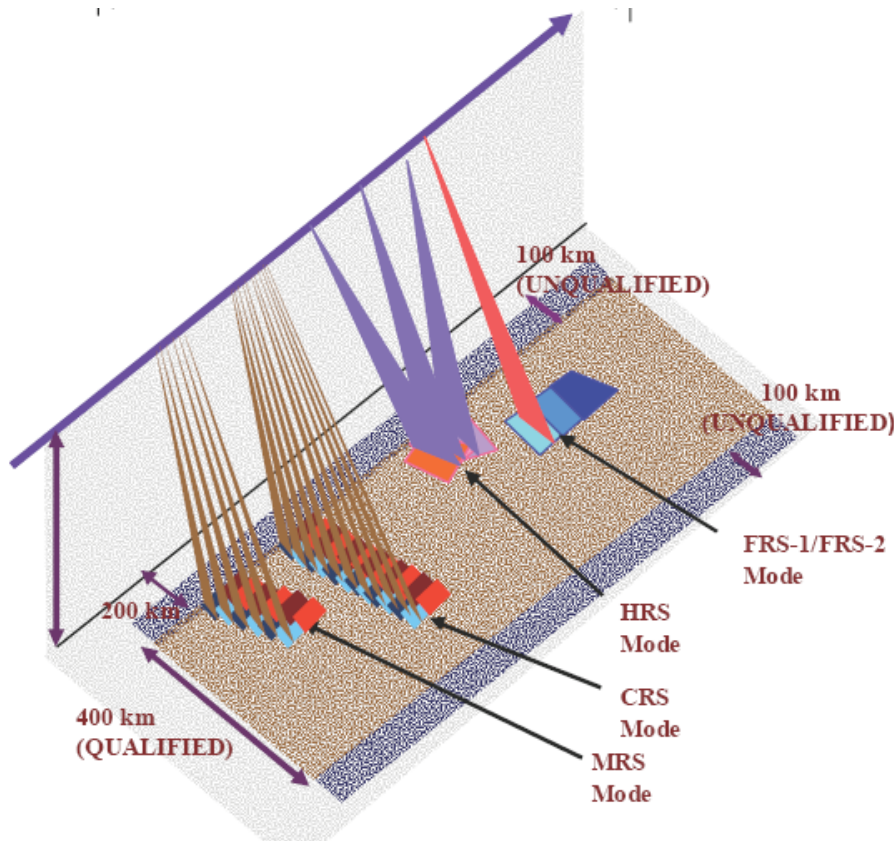


Figure 1: Schematic Diagram showing different beam modes of RISAT-1 SAR

Table1: RISAT-1 Image quality parameters

Swath coverage	Selectable within 107–659 km off-nadir distance on either side			
Incidence angle coverage	12°–55°			
Image quality				
Mode		Polarization		
	Single pol	Dual pol	Circular (hybrid)	Quad pol
	HH/HV/VV/VH	HH + HV/VV + VH	polarimetry	HH + HV + VV + VH
			TX: CP	
			Rx: V and H	
			(experimental)	
HRS	1 m (azimuth) × 0.67 m (range) resolution, 10 × 10 km (10 × 100 km experimental) spot, Min $\sigma_0 = -16$ dB			
FRS-1	3 m (azimuth) × 2 m (range) resolution, 25 km swath, Min $\sigma_0 = -17$ dB			
FRS-2			3 m (azimuth) × 4 m (range) resolution, 25 km swath, Min $\sigma_0 = -19$ dB	9 m (azimuth) × 4 m (range) resolution, 25 km swath, $\sigma_0 = -20$ dB
MRS	21–23 m (azimuth) × 8 m (range) resolution, 115 km swath, Min $\sigma_0 = -17$ dB			
CRS	41–55 m (azimuth) × 8 m (range) resolution, 223 km swath, Min $\sigma_0 = -17$ dB			

HRS: High resolution stripmap, FRS: Fine resolution stripmap, MRS: Medium Resolution ScanSAR, CRS: Coarse resolution ScanSAR, C-HRS, C-FRS, C-MRS and C-CRS refers to circular polarization in respective modes.

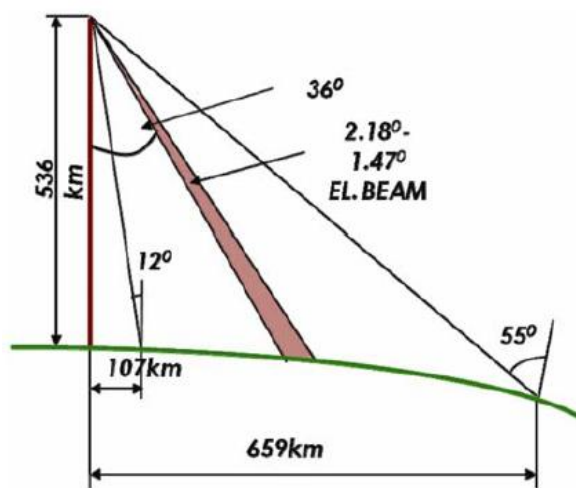


Figure 2: Imaging Geometry of RISAT-1

This C-band active antenna based, multi-mode SAR payload was launched on 26th April 2012 by PSLV-C19 flight. After positioning at 536 km sun-synchronous dawn-dusk circular orbit it was operated on May 1, 2012. RISAT-1 mission is designed to provide SAR images

with a repetivity period of 24 days. Its orbit design takes the space craft crossing the equator in its descending path (north to south) at 6 AM and crosses the equator in its ascending path (south to north) at 6 PM. RISAT- 1 SAR sensor transmits a series of electromagnetic pulses of radiation in C band using an active array antenna of 576 transmit receive modules mounted in panel of ~6m X 2m. The electromagnetic pulses strike the earth surface and the backscattered signal is received by the receive modules mounted in the antenna and by time correlated processing of this signal, information about the earth surface is deciphered.

2.0 Theoretical background

In general, the antenna gain profile, measured on ground facility, is well calibrated and accurate, but sometimes due to large size of antenna, thermal stresses and spacecraft body, the pattern in flight may deviate from one measured on ground. On board calibration methods do not provide measurement for such deviations. Also, the final product from SAR sensor is processed with special signal processing algorithms such as SAR range and azimuth processing. Such processing also modifies the radiometry of the output and needs to be calibrated. This is achieved by ground calibration using standard targets. A standard target is a target with a known Radar cross section.

Radar Scattering Cross-section: The strength of the radar signal reflected from an object is conventionally represented by the radar cross-section (RCS) σ . It is expressed in terms of the physical size of an isotropic radiator that would give rise to the same level of reflection as that observed from the sample target. The RCS, σ is essentially a measure of target's ability to reflect radar signals in the direction of the radar receiver and has units of area (m^2), or when expressed in decibels as dBm^2 . RCS is usually used for point targets or targets comparable to the resolution cell. In remote sensing, applications involve extended targets that usually are much larger than a resolution cell of the radar. Therefore, it is appropriate to define a differential scattering coefficient as the radar cross-section per unit area. The differential coefficient, σ^o (generally referred to as just scattering coefficient) is defined as the average value of scattering cross-section per unit area:

$$\sigma^o = \langle \sigma | \Delta A \rangle \quad (1)$$

where ΔA is the area on the ground having a radar cross-section of σ . In general, σ^o has significant variation with incidence angle, wavelength, polarization and the properties of the scattering surface itself.

For a given SAR image, the digital number (DN) is proportional to the received voltage [16]. Therefore, the image intensity I , is proportional to the received power P_r . The process to retrieve SAR backscattering coefficient from the observed SAR image intensity is known as radiometric calibration [11]. Radiometric calibration procedure provides a reference mechanism between SAR DN values and known Radar Cross Section (RCS) of a deployed standard target or distributed target [12-14].

Amazon Rainforest is an established distributed target for SAR data calibration as announced by SAR subgroup of Working Group on Calibration and Validation (WGCV) of Committee on Earth Observation Satellite (CEOS). Canadian Boreal forest is also being used by researchers as distributed target for SAR calibration [15, 16]. There are various standard point targets for SAR data calibration which can be classified based on their nature of functionality viz. active and passive standard targets. In active domain, active radar calibrator (ARC) and polarimetric active radar calibrator (PARC) are used whereas in passive domain dihedral corner reflector (DHCR), triangular trihedral corner reflector (TTCR), square trihedral corner reflector (STCR), luneburg lens are used. In this study, passive standard target (TTCR) has been utilized for RISAT-1 SAR calibration. For absolute calibration, point target RCS is computed and compared with the theoretical RCS of CR. For RCS computation the widely used methods are [17]:

1. Peak estimation method and
2. The integral method

In integral method, the value of calibration constant is derived by integrating the power from all the pixel values of point target where as for peak estimation method estimated peak value of a reflector is used [14, 17, 18].

Gray et al. (1990) [17] showed that integral method for SAR image calibration is better than the peak estimation method. SAR image calibration where the peak pixel value of the impulse response of a known radar reflector is used to derive the backscatter coefficient of adjacent clutter areas may be affected from the problems arising from coherent and non-coherent radar or processor phase errors with associated focus problems, look registration, and underestimation of the peak value of the reflector. It was shown by them [17] that the integral method is independent of the radar system focus or partial coherence and thereby possesses an important advantage over the usual technique which relies on an estimate of the peak of the reflector impulse response. The impulse response function (IRF) is the point target return which measures the focusing and energy distribution in SAR image in both elevation and azimuth direction. As it has already been proven that integral method is better

than peak estimation method, hence, in this work, integral method has been used for deriving the calibration constant.

Calibration and monitoring of SAR instruments parameters with respect to different beams and polarizations is required to ensure the consistency in the derived backscattered values. Use of passive corner reflectors as point targets is one of the fundamental approaches for SAR calibration. To evaluate the image quality parameters, impulse response of these reflectors in both elevation and azimuth directions is measured. The image quality parameters evaluated are background to peak ratio (BP) ratio, peak side lobe ratio (PSLR) , spatial resolution, radiometric resolution and integrated side lobe ratio (ISLR) for each of the corner reflectors (shown in figure 3 [19]).

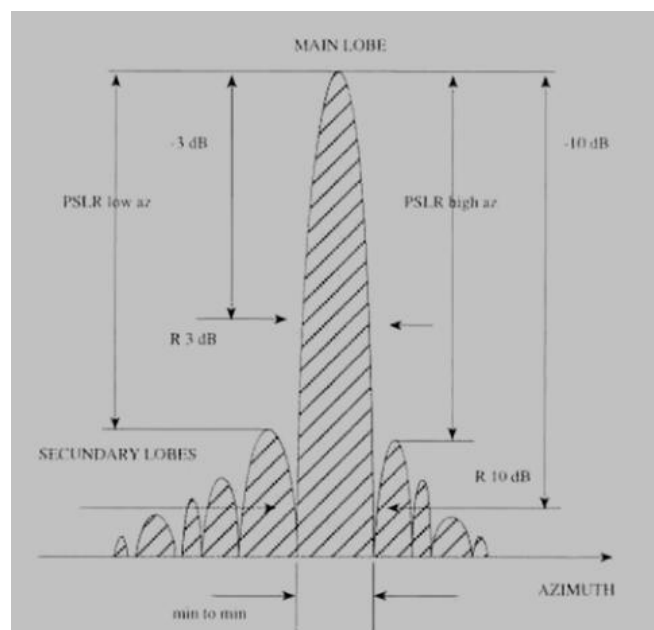


Figure 3: Graphical representation of a SAR point target showing several quality parameters

Spatial Resolution

The spatial resolution is the distance between the points with intensities 3dB below the maximum intensity of the main lobe peak in the azimuth and range directions. The definition of the 3dB points is equivalent to the points with half the intensity of the maximum.

Peak side lobe ratio

The peak side lobe ratio, PSLR, is defined as the ratio of the peak intensity of the most prominent side lobe to the peak intensity of the main lobe. There are two measures of the PSLR, corresponding to the two sides of the main lobe both in azimuth and range directions. This parameter is expressed in decibels.

Integrated side lobe ratio

The integrated side lobe ratio, ISLR, is the ratio of the power (energy) in the main peak to the total power in all the side lobes. As for the PSLR, the ISLR is a measurement of the relative importance of the side lobes with respect to the main lobe.

Radiometric Resolution

The radiometric resolution is a measure of the ability of the system to discriminate, or resolve, areas of different scattering properties. Meanwhile the geometric resolution is a quantitative measure of the ability of the system to discriminate different objects in space, the meaning of radiometric resolution is to quantify the minimum distance between two reflectivity levels (in a homogeneous zone) which can be separated by the radar [24].

The radiometric analysis is the counterpart in the frequency domain of the IRF analysis. The targets of investigation are uniform, extended regions, which ideally have a pointlike signature in the frequency domain. In fact, the radiometric resolution quantifies "the ability to distinguish between uniformly distributed targets with different backscattering coefficients". This ability is strongly related to the phenomenon of speckle and therefore to the image multi-looking [25].

The radiometric resolution is dependent on signal, speckle, and thermal noise intensities [24]. A conventional definition for the radiometric resolution is [26]:

$$\gamma = 10 \log_{10} \left(1 + \frac{\sigma}{\mu} \right) \quad (1.1)$$

where μ and σ are the mean value and standard deviation of the distributed target intensity values.

Ambiguities and Ghosts in SAR images

Ambiguities are the manifestation of ‘ghosts’ (undesired) targets in the SAR images inherent to pulsed radar systems [27]. They are intrinsic effects of a SAR system, both in azimuth and range. There are two types of ambiguities in SAR: the range ambiguities, and the azimuth ambiguities. The range ambiguities arise when different backscattered echoes, one related to a transmitted pulse and the other due to a previous transmission, temporarily overlap during the receiving operation (Figure 3.1). In this case the range information contained in the echo delay becomes ambiguous because it cannot be directly related to a single transmitted pulse. This effect is particularly relevant for spaceborne sensors due to the relatively large target-sensor range [28]. As the range ambiguities result from simultaneous arrival of different pulses at the antenna, they are controlled via the PRF (Pulse Repetition Frequency) selection

[19]. An upper limit to the PRF is set by the necessity to avoid that successive echoes backscattered by the illuminated scene are received simultaneously. This is achieved if the time extension of each echo is smaller than the interval between two successive pulses [28]. Furthermore, as every antenna pattern, the range direction has sidelobes. Such lobes can allow (when in presence of special combination of sidelobes position and reception window) the reception of echoes coming from portions of the earth outside the range (with the creation of range ghosts) [24] (Figure 3.2). Such phenomenon can be avoided with a proper selection of the antenna and reception window parameters [19].

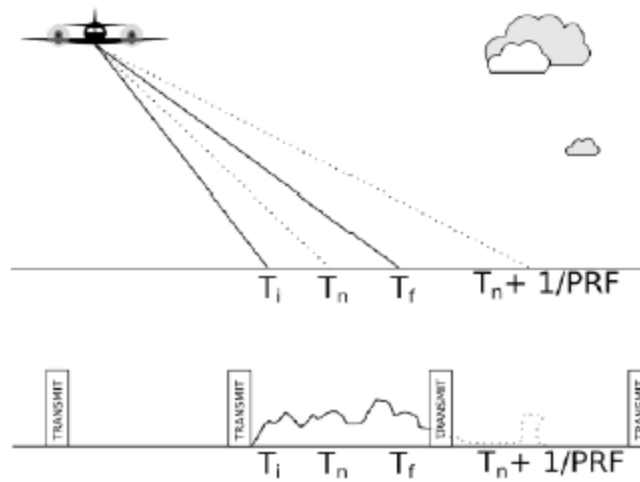


Figure 3.1: Range ambiguities arise because of a bad configuration of the PRF

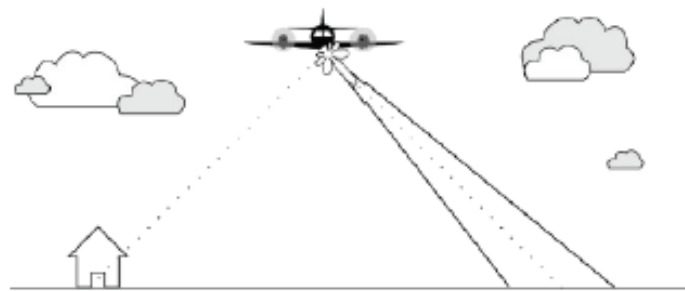


Figure 3.2: Range ambiguities arise because of antenna pattern sidelobes

The azimuth ambiguities are caused by the aliasing of the Doppler phase history of each target that is sampled according to the sensor azimuth sampling frequency, f_{sa} , which equals the Pulse Repetition Frequency (PRF). Usually, such ambiguities are kept below a reasonable level by exploiting the Azimuth Antenna Pattern (AAP), that acts as a sort of anti-alias pre-filter, by illuminating ground patches in the direction of the desired contributions and

blocking returns from "interfering" angles [29]. These ambiguities appear because of the sidelobes of the antenna pattern in azimuth direction. This effect is particularly relevant for high reflectivity objects that appear in the SAR image as ghosts targets inside low reflectivity areas [24].

Ambiguity level (ratio)

The ambiguity level is the ratio of the energy in the ghosts to that in the main lobe, and is expressed in dB [19]. Curlander and McDonough [25] defined the same concept as the ambiguity to signal ratio (ASR).

$$ASR = 10\log_{10} \left(\frac{Ambiguity}{PointTarget} \right) \tag{1.2}$$

where *Ambiguity* and *Point Target* are the peak power of the ghost and of the actual target respectively.

To check the form of the impulse response, point targets such as trihedral corner reflectors, with a large RCS are often used. For such targets, the radar backscatter does behave like a Dirac delta function (under certain viewing geometries) and the radar returns can be considered completely coherent. The large RCS is required to ensure adequate visibility above the surrounding background scatterers, often termed clutter. One measure of visibility is the target signal-to-clutter ratio [20]:

$$SCR = \frac{\sigma_{pq}^T}{\langle \sigma_{pq}^C \rangle} \tag{2}$$

where σ_{pq}^T is the point target RCS and $\langle \sigma_{pq}^C \rangle$ the average background clutter RCS. To measure the target signal-to-clutter ratio from an actual SAR image, the ratio of the peak power in the target impulse response to the mean background clutter power, estimated from an area located close to the target, is often used.

Peak Intensity and Amplitude

A SAR image is the result of coherently processing returned echo signal, thus the pixel values are complex quantities. For most applications the representation of the magnitude of the image is enough. It is possible to use the modulus of the complex pixel (amplitude) as well as the squared modulus (intensity). The peak intensity is the maximum pixel value in the main lobe of the impulse response function (if the image has been power detected). The square root of the intensity is amplitude.

3.0 Study Area and Data sets

Corner reflectors deployment was carried out over the grounds of Bopal cal-val site and SAC campus ground in Ahmedabad identified for the calibration purpose. A total of 3 (three) data sets of RISAT-1, MRS mode and two scenes of FRS-1 mode were acquired for the purpose. Figure 4a and 4b show the location of Bopal cal-val ground and SAC ground respectively on Google Earth image. Corner reflector deployment details are shown in Table 2a and 2b for FRS-1 and MRS nodes respectively.



Figure 4a: Location of Bopal cal-val site
(Courtesy: Google Earth)



Figure 4b: Location of SAC ground
(Courtesy: Google Earth)

Table 2a: Details of corner reflector deployment for FRS-1 and different beam modes

S. No.	Site	Date	Beam	Incidence Angle	Orbit	Polarization, Node, Look Direction	No. Of deployed Corner reflector
1.	Bopal cal-val site, Ahmedabad	21st April 2015	104	44.780	16447	HH, HV Ascending, Left look	1
2.	SAC ground, Ahmedabad	21 st April 2015	104	44.780	16447	HH, HV Ascending, Left look	2
3.	Bopal cal-val site, Ahmedabad	25 th April 2015	21	31.209	16507	HH, HV Ascending, Right look	1

Table 2b: Details of corner reflector deployment for MRS

S. No.	Site	Date	Beam	Incidence Angle	Orbit	Polarization, Node, Look Direction	No. Of deployed Corner reflector
1.	Bopal cal-val site, Ahmedabad	10 th June 2015	87-97	36.821	17193	HH, HV Descending, Left look	1
2.	Bopal cal-val site, Ahmedabad	5 th July 2015	87-97	36.796	17570	HH, HV Descending, Left look	1
3.	Bopal cal-val site, Ahmedabad	30 th July 2015	87-97	36.799	17947	HH, HV Descending, Left look	1

4.0 Methodology

The most common image quality parameters measured from SAR images are derived from and describe the shape of the impulse response function. The impulse response function (IRF) of a SAR image is the response to a point target assuming negligible reflectivity and thermal noise. The IRF is also sometimes referred to as a point spread function. For absolute calibration RCS of corner reflector is computed and compared with the theoretical RCS.

For point target analysis, passive corner reflectors of known radar cross-section were deployed considering three important points [30]:

- (i) Orientation of corner reflector with respect to SAR antenna
- (ii) The deployment site characteristics and
- (iii) Size and material of the CR i.e. it should have sufficient energy for scattering.

Precise deployment of CR is the primary requirement and for the best results, CR should be pointed directly along the bore sight of the SAR antenna [31]. Secondly, deployment site should be free from the multi-path contributions and should be located distant from the power lines and housing colonies [32].

After receiving single look complex (SLC) data of FRS and ground range detected product (GRD) of MRS, reflectors were located in image as shown in Figure 5. Integral box method [17] was applied using Gamma software to derive calibration constant. In integral method, power from a standard point target is taken by integrating the power from all pixel values corresponding to the point target, to arrive at the calibration constant.

In order to arrive at the interpolated integrated power from the point target, two directional interpolation is done on the power image with an interpolation factor $f_{int}(=16)$ in range and azimuth direction to get point target IRF as shown in Figure 3. Integrated power from two dimensional impulse responses is analyzed for estimating main lobe and side lobe energy received from the point target. The image interpolation is done in frequency domain by FFT. The FFT of the sub image surrounding the point target is interpolated f_{int} times in frequency domain and then inverse FFT is performed to obtain interpolated data.

The back scattering coefficient of a target is determined by [21]

$$\sigma^0 = \left(\frac{1}{N} \sum_{i,j=1}^{i,j=N} DN_{i,j}^2 \right) \frac{1}{K} \frac{\sin \alpha}{\sin \alpha_{ref}} \quad (3)$$

where, N is the number of pixels within the area of interest (here $N = 7$ for MRS data, low value of N is taken to avoid the effect of building near to the location of corner reflector and $N=32$ for FRS data), i and j are the range and azimuth locations of the pixel within the distributed target containing N pixels, DN_{ij} is the digital number corresponding to the pixel at location (i,j) , α is the average incidence angle within the distributed target, α_{ref} is the reference incidence angle, and K is the absolute calibration constant determined by [22] :

$$K = \frac{I_p P_{Agr} \sin \alpha}{\sigma} \quad (4)$$

σ is the radar cross section of reflector. P_{Agr} is ground range pixel area in square meter, α is incidence angle at target position and I_p is back ground corrected integrated power of the target IRF (Impulse Response Function).

Following are the steps for the calculation of background corrected integrated power using corner reflectors as point target [23]:

1. Extraction of a sub image of $M \times M$ pixels (here $M=7$ for MRS and $M=32$ for FRS mode data) around the point target from image converting the pixel values into intensity by squaring pixel DN values and calculation of the integrated power (P_I).
2. Selection of four corner areas around the point target in sub image with $N \times N$ (here $N=2$ for MRS and $N=8$ for FRS mode data) pixels (as shown in Figure 5) and derivation of the mean background intensity and calculation of the mean background power ($\langle B \rangle$).
3. Subtraction of the mean background power from the integrated corner reflector power value to obtain background corrected integrated power (P_T).

$$P_T = P_I - \langle B \rangle \quad (5)$$

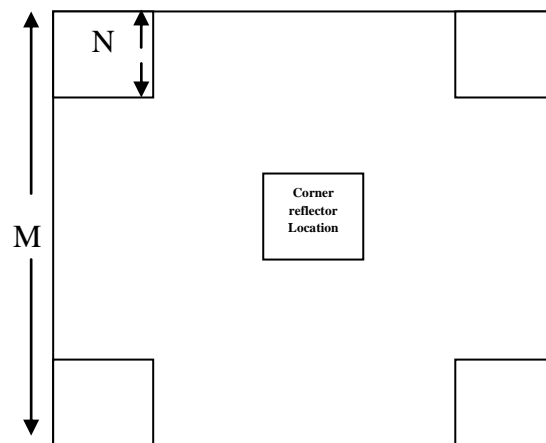


Figure 5: Subset of the image containing corner reflector

5.0 Results and Discussions

Corner reflectors have been used to carry out calibration of RISAT-1 SAR data. Figure 6 shows the deployed corner reflectors. Reflector responses in RISAT-1 SAR images were analysed to derive radiometric parameters of the data and computing the necessary calibration parameters. Figures 7.1 and 7.2 show the response of the reflectors captured in the RISAT-1 SAR, MRS and FRS images respectively.



Figure 6: Trihedral Corner reflector deployed in Bopal cal-val site

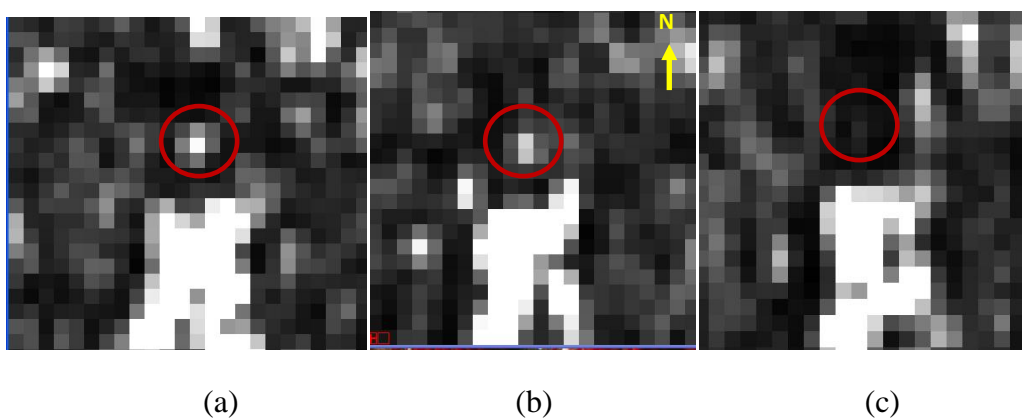
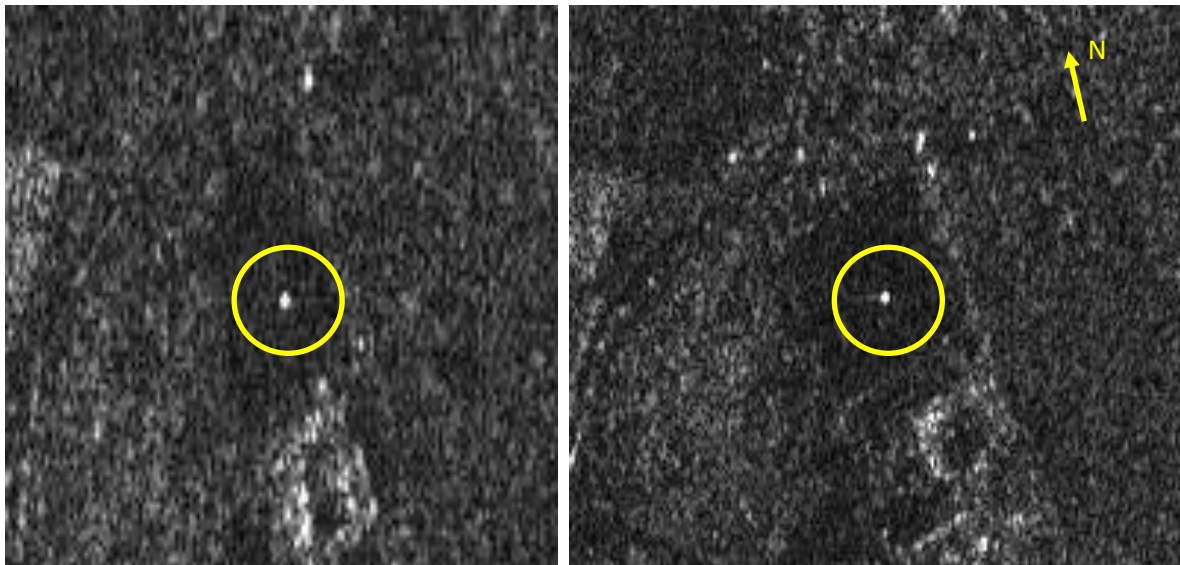


Figure 7.1: Reflectors seen in RISAT-1 MRS image of (a) 5th July 2015 (b) 30th July 2015 and (c) 10th June 2015



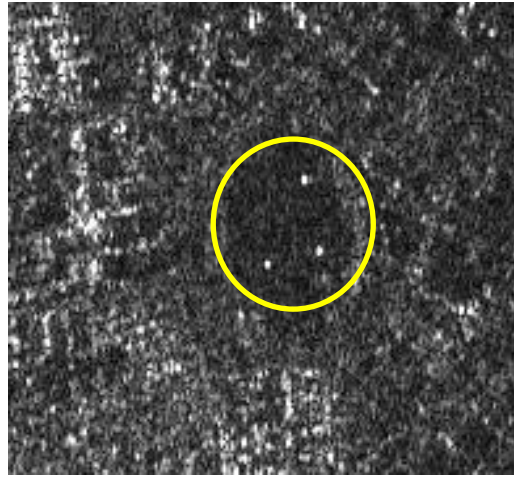
Figure 7.1d: Image showing the background variations of the site and moisture in the soil on 30th July 2015

It can be seen from Figure 7.1 b that the brightness variations in the field is quite high, as it rained on 30th July so there was moisture in the soil. Also, because of the uneven height variations of the vegetation on that day, volume scattering occurred. Due to the soil moisture and background roughness, brightness of the background increased and the same was reflected in the image of 30th July 2015. The response of the corner reflector could not be seen in 10th June 2015 image (Figure 7.1 c) due to the improper orientation of the CR.



(a)

(b)

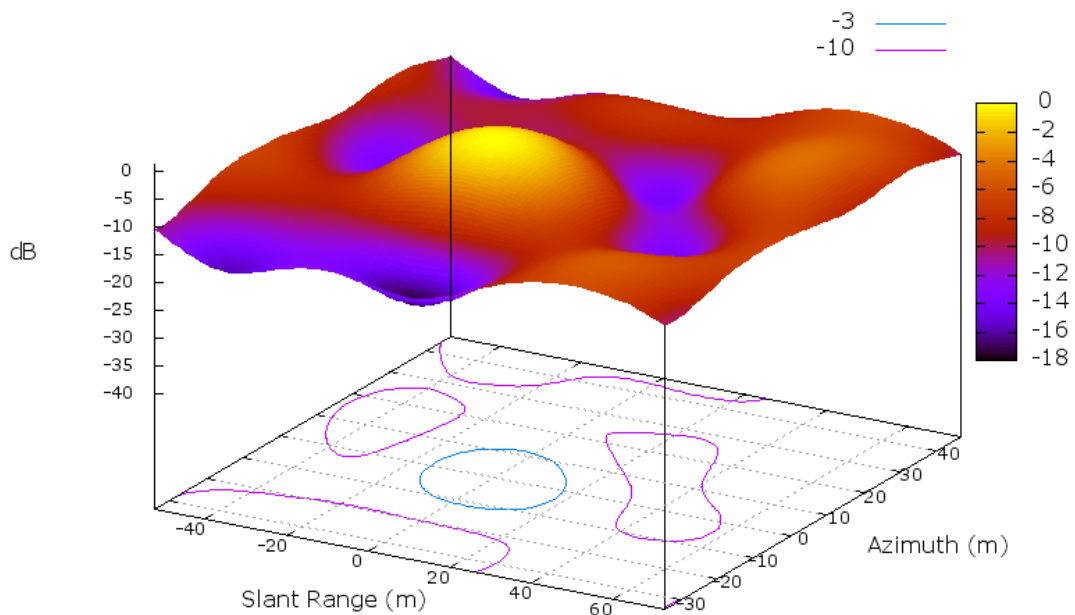


(c)

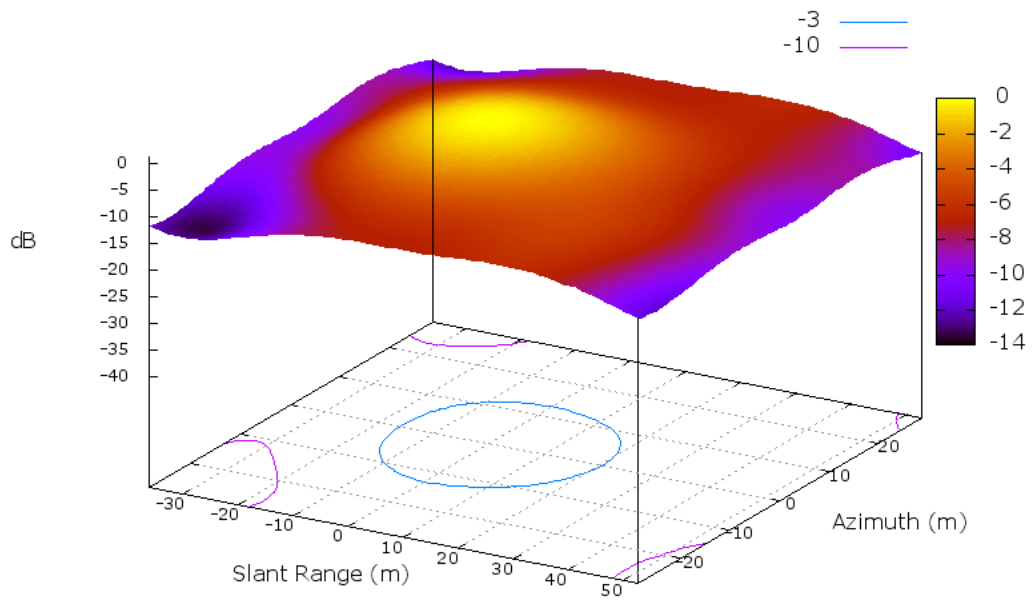
Figure 7.2: Reflectors installed in Bopal cal-val site as seen in RISAT-1 FRS1 image of (a) 25th April 2015 (b) 21st April 2015 (c) Reflectors installed in SAC ground as seen in RISAT-1 FRS1 image of (a) 21st April 2015

Integrated power from two dimensional impulse responses has been analysed after removing clutter noise for the standard target. From point target impulse response, apart from deriving calibration constants, range and azimuth spatial resolution, range and azimuth peak side lobe ratio (PSLR), ISLR, Background to peak ratio have been computed. From the interpolated response of the point target, firstly, calibration constant was derived and then the data quality parameters were obtained.

Figure 8 and Figure 9 show the impulse response for point targets in MRS, HH and FRS1, HH data respectively.

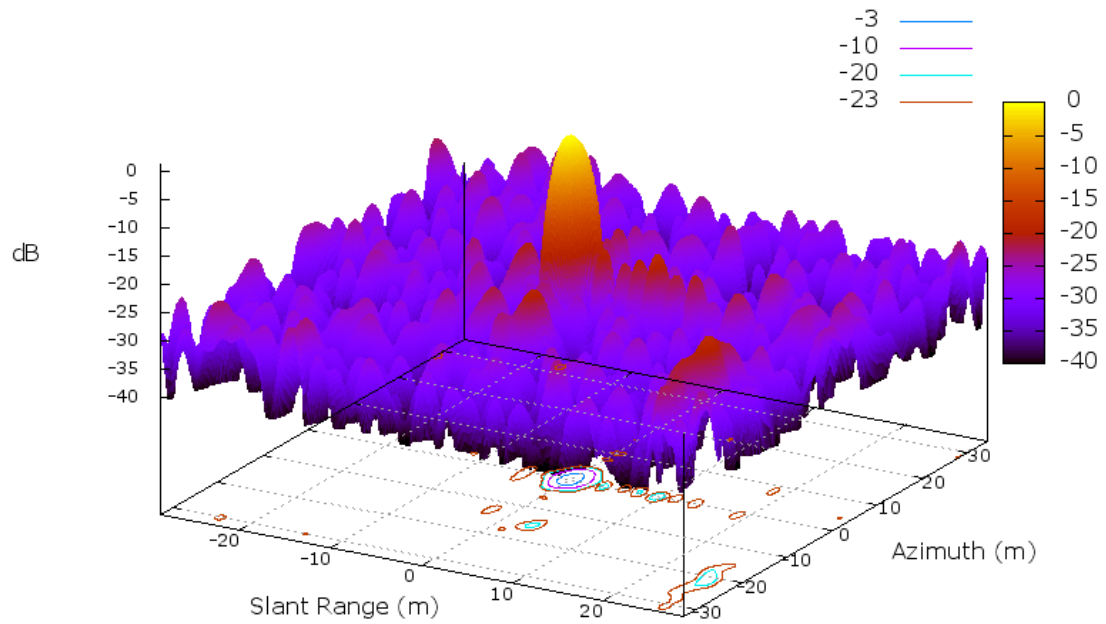


(a)

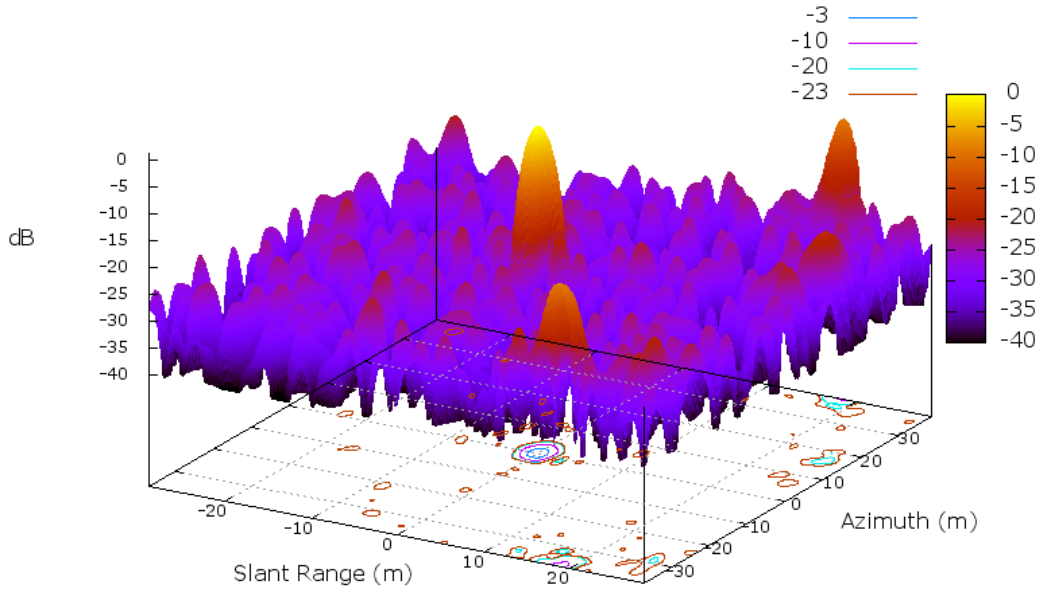


(b)

Figure 8: Point target Impulse response function for point target installed in Bopal Cal-Val site for MRS-HH data of (a) 5th July 2015 (b) 30th July 2015

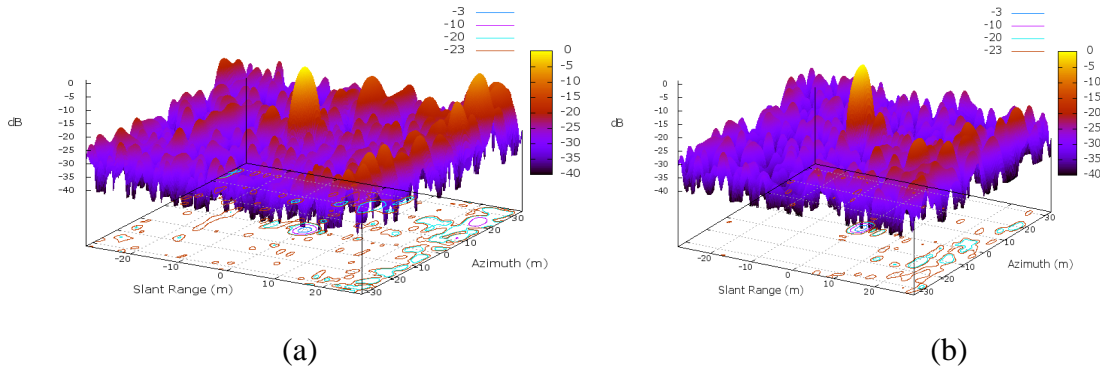


(a)



(b)

Figure 9.1: Point target Impulse response function for point target installed in Bopal Cal-Val site for FRS-HH data of (a) 21st April 2015 (b) 25th April 2015



(a)

(b)

Figure 9.2: Point target Impulse response function for the two point targets installed in SAC ground for FRS-HH data of 21st April 2015

The peak value of the power corresponds to the point target (CR) installed. The effect of the building situated near to the CR is clearly seen. Only HH polarization data was analysed, point target analysis for HV polarization was not carried out in the study due to the weak return energy from the corner reflectors, as the type of corner reflectors (tri-hedral) deployed are effective for co-polarization and circular polarization channels only.

The calibration constants derived using the methodology explained in the previous section and its comparison with the calibration constant values given in the header file

(BAND_META.txt file) are shown in Table 3 and Table 4a ,4b for MRS and FRS data respectively.

Table 3a: Comparison of the estimated and provided calibration constant for RISAT-1 MRS mode

Date of Pass	Node	Beam	Calibration Constant Estimated from the study (HH) (dB) (A)	Calibration Constant from Header (dB) (B)	Difference (dB) (A-B)
30-Jul-15	Descending	10 (87-97)	72.7115	72.327	
05-Jul-15	Descending	10 (87-97)	71.3395	72.231	
		Average	72.0255	72.279	0.2535

Table 4a: Calibration constant estimated for FRS data of 21st April 2015	
Beam No. 104, HH	
Point Target	Calibration Constant (dB)
Bopal_CR1	74.9463
SAC_CR1	76.9413
SAC_CR2	77.3631
Average	76.4169
Calibration Constant from Header	78.178
Difference	1.7611

Table 4b: Calibration constant estimated for FRS data of 25th April 2015	
Beam No. 21, HH	
Point Target	Calibration Constant (dB)
Bopal_CR1	72.3510
Average	72.3510
Calibration Constant from Header	73.199
Difference	0.848

Image quality parameters computed for MRS and FRS data are shown in Table 5 and 6 respectively.

Table 5: Estimated image quality parameters for FRS data dated 21st April 2015

Image Quality Parameters for SAC_CR1		Image Quality Parameters for SAC_CR2	
-3 dB width		-3 dB width	
Range	2.398	Range	1.913
Azimuth	3.932	Azimuth	4.329
Peak to side lobe ratio (PSLR) (dB):		Peak to side lobe ratio (PSLR) (dB):	
Range	-16.316	Range	-15.357
Azimuth	-19.076	Azimuth	-21.732
Integrated side lobe ratio (ISLR) (dB):		Integrated side lobe ratio (ISLR) (dB):	
Range	0.02	Range	0.021
Azimuth	0.01	Azimuth	0.002

(a)

Image Quality Parameters for BOPAL_CR	
-3 dB width	
Range	2.272
Azimuth	5.196
Peak to side lobe ratio (PSLR) (dB):	
Range	-14.614
Azimuth	-21.548
Integrated side lobe ratio (ISLR) (dB):	
Range	0.02
Azimuth	0.007

(b)

Table 6: Estimated image quality parameters for MRS data dated

Image Quality Parameters for BOPAL_CR	
-3 dB width	
Range	41.482
Azimuth	26.221
Peak to side lobe ratio (PSLR) (dB):	
Range	-8.793
Azimuth	0.243

(a): 30th July 2015

Image Quality Parameters for BOPAL_CR	
-3 dB width	
Range	35.333
Azimuth	22.678
Peak to side lobe ratio (PSLR) (dB):	
Range	-6.767
Azimuth	-7.677

(b): 5th July 2015

It can be seen from Table 5 that the calibration constants estimated differs from the values given in the header file by less than 1 dB for MRS mode whereas, for FRS beam 104 the difference is less than 2dB and for FRS beam 21 the difference is again less than 1dB. Average values for PSLR in range for 21st April FRS HH data was found as -15.42 dB and -20.78 dB in the azimuth direction. Maneesha Gupta *et al* , 2015 [30] reported the values of PSLR in range and azimuth as -19 and -24 dB respectively.

6.0 Future Work

Following work has been planned in the near future:

1. Processing and analysis of other dates MRS HH data and estimation of calibration constant.
2. Validation of the calibration constant estimated from the study using the RCS calculation approach.

3. Geometric calibration has also been planned using DGPS.
4. Phase calibration using Active Radar Calibrator (ARC)*.
 - Arc will be provided by MRSA, SAC for the study.

Acknowledgements:

Authors are extremely grateful to Shri Tapan Misra, Director, Space Applications Centre, for his encouragement to carry out the work. Support extended from Dr. P K Pal, DD-EPISA and Dr. B K Gohil, GD-ADVG, EPISA are sincerely acknowledged. Authors also thank Dr K Kotecha, Director, Institute of Technology, Nirma University, Ahmedabad for his continuous support during research work. Authors are highly grateful to Shri Ramanujam and Shri Amit Shukla for sparing their precious time to share technical views on various points during the study.

References

- [1] C. A. Wiley, "Pulsed doppler radar methods and apparatus," **US**. Patent 3,196,436, filed Aug. 13, 1954, patented July 20, 1965.
- [2] W. T. K. Johnson, "Magellan Imaging Radar Mission to Venus," *Proc. IEEE*, vol. 79, no. 6, pp. 777-790, June 1991.
- [3] E. P. W. Attema, "The Active Microwave Instrument On-Board the ERS-1 Satellite," *Proc. IEEE*, vol. 79, no. 6, pp. 791-799, June 1991.
- [4] Y. Nemoto, H. Nishino, M. Ono, H. Mizutamari, K. Nishikawa, and K. Tanaka, "Japan Earth Resources Satellite-1 Synthetic Aperture Radar," *Proc. IEEE*, vol. 79, no. 6, pp. 800-809, June 1991.
- [5] R. L. Jordan, B. L. Huneycutt, and M. Werner, "The SIR-CIX-SAR Synthetic Aperture Radar System," *Proc. IEEE*, vol. 79, no. 6, pp. 827-838, June 1991.
- [6] R. K. Raney, A. P. Luscombe, E. J. Langham, and S. Ahmed, "RADARSAT," *Proc. IEEE*, vol. 79, no. 6, pp. 839-849, June 1991.
- [7] C. Elachi, E. Im, L. E. Roth, and C. L. Werner, "Cassini Titan Radar Mapper," *Proc. IEEE*, vol. 79, no. 6, pp. 867-880, June 1991.
- [8] Tapan Misra, S. S. Rana, N. M. Desai, D. B. Dave, Rajeevjyoti, R. K. Arora, C. V. N. Rao, B. V. Bakori, R. Neelakantan and J. G. Vachchani, "Synthetic Aperture Radar payload on-board RISAT-1: configuration, technology and Performance", *CURRENT SCIENCE*, VOL. 104, NO. 4, 25 FEBRUARY 2013.
- [9] "Earth Observation System report," NASA, Washington, DC, Synthetic Aperture Radar Instrument Panel Rep., vol. IIf, 1987.
- [10] Anonymous, "RISAT-SAR Payload DDR Document: SAC/RISAT/DDR/01/2009, Space Applications Centre, Ahmedabad, 2009.
- [11] John C. Curlander, Robert N. McDonough, "Synthetic Aperture Radar Systems and Signal Processing", 1991, Wiley Series in Remote Sensing.
- [12] M Dobson, F Tulaby, D Brunfeld, and D Held, "External calibration of SIR – B imagery with area extended point targets", 1986, *IEEE Trans. Geosci. Remote Sensing*, vol. GE 24, No.4, pp. 453 – 461.
- [13] A D Woode, Y L Densnos, and H Jackson, "The development and first results from the ESTEC ERS-1 Active Radar Calibration unit", 1992, *IEEE Trans. Geosci. Remote Sensing*, Vol. 30, No.6, pp. 1122-1130.
- [14] Rosich B., Meadows P., "Absolute Calibration of ASAR Level 1 Products Generated with PF – ASAR" 2004, Technical Note, ESA, ESRIN.

- [15] S Srivastava, S Cote, S Muir, and R Hawkins, “The RADARSAT-1 imaging performance, 14 years after launch, and independent report on RADARSAT-2 image quality”, 2010, IEEE, Geoscience and Remote Sensing Symposium (IGARSS), pp. 3458 – 3461, doi:10.1109/IGARSS.2010.5650129
- [16] R Hawkins, E Attema, R Crapolicchio, P Lecomte, J Closa, P J Meadows, “Stability of Amazon Backscatter at C-Band: Space borne Results from ERS-1/2 and RADARSAT-1.”, 2000, SAR Workshop: CEOS Committee on Earth Observation Satellites; Working Group on Calibration and Validation, Proceedings of a Conference held 26-29 October 1999, Toulouse, France. Edited by Robert A. Harris and L. Ouwehand. Publisher: Paris: European Space Agency, ESA-SP vol. 450, ISBN: 9290926414, p.99.
- [17] Gray A. L., Vachon P. W., Livingstone C. E. and Lukowski T. I, “Synthetic Aperture Radar calibration using reference reflectors”, IEEE Transactions on Geoscience and remote sensing, vol. 28, No. 3, pp: 374 - 383, 1990.
- [18] Mohan S., Basu S. K., Jha A. M., Mishra Tapan, Kewalia R. K., (1995), Calibration of ERS-1 SAR Data', Scientific report, SAC/RSA/RSAG/ERS-1/SN/07/95.
- [19] A. Martinez and J.L. Marchand, “SAR image quality assessment”, Revista de Teledeteccion, 1993.
- [20] Anthony Freeman, “SAR calibration: An overview”, IEEE Transactions on geoscience and remote sensing, vol. 30, No. 6, pp: 1107-1121, 1992.
- [21] Laur H., (1992), ERS-1 SAR Calibration: Derivation of Backscattering Coefficient in ERS-1 SAR PRI Products, ESA/ESRIN, Issue 1, Rev. 0.
- [22] ESA Document, (2004), Absolute Calibration of ASAR Level 1 Products Generated with PF-ASAR, Issue 1, Rev. 5.
- [23] Gupta M., B. Kartikeyan and S. Chowdhury, (2014), An approach to evaluate and monitor RISAT-1 SAR from level-0 raw data. International Journal of Remote Sensing, <http://dx.doi.org/10.1080/01431161.2014.943323>.
- [24] G. Franceschetti and R. Lanari, Synthetic Aperture RADAR PROCESSING. Electronic engineering systems series, CRC Press, 1999.
- [25] J. C. Curlander and R. N. Mc Donough, Synthetic Aperture Radar: Systems and Signal Processing. Wiley, John & Sons, 1991.
- [26] P. Oliver and D. Vidal-Madjar, “Empirical estimation of the ERS-1 SAR radiometric resolution,” Int. J. Remote Sens., vol. 15, no. 5, pp. 1109–1114, 1994.
- [27] A. Freeman, “On ambiguities in SAR design,” tech. rep., Jet Propulsion Laboratory (JPL) - California Institute of Technology, 2006.
- [28] G. Franceschetti, R. Lanari, and P. V., “Wide angle SAR processors and their quality assessment,” in IGARSS 91, pp. 287 – 290, 1991.

[29] A. M. Guarnieri, "Adaptive removal of azimuth ambiguities in sar images," IEEE Transactions on Geoscience and Remote Sensing, vol. 43, no. 3, pp. 625–633, 2005.

[30] Maneesha Gupta, Anuja Sharma and B. Kartikeyan, "Image quality assessment of RISAT-1 SAR using trihedral corner reflectors in different beams", Journal of Geomatics, Vol.8, No.2, pp:130-139, October 2014.

[31] Norris J., P.W. Vachon, D. Schlingmeier, R. English and L. Gallop (2004). Expendable trihedral corner reflectors for target enhancement and position control in RADARSAT-1 fine beam mode SAR imagery: Results from an exercise Narwhal Pre-Trial Deployment defence R&D Canada-Ottawa TECHNICAL MEMORANDUM DRDC Ottawa TM 2004-197 September 2004.

[32] Donald, M. Ugsang, K. Honda and G. Saito (2001). Assessment of small passive corner reflectors for geometric correction of RADARSAT fine beam mode SAR data. 22nd Asian conference on Remote Sensing, 5-9 November 2001, Singapore.